

Estimation of 3D active earth pressure under nonlinear strength condition

D.B. Zhang¹, Y. Jiang² and X.L. Yang^{*2}

¹Work Safety Key Lab on Prevention and Control of Gas and Roof Disasters for Southern Coal Mines, Hunan Provincial Key Laboratory of Safe Mining Techniques of Coal Mines, Hunan University of Science and Technology, Xiangtan 411201, China

²School of Civil Engineering, Central South University, Hunan 410075, China

(Received January 2, 2019, Revised March 4, 2019, Accepted March 5, 2019)

Abstract. The calculation of active earth pressure behind retaining wall is a typical three-dimensional (3D) problem with spatial effects. With the help of limit analysis, this paper firstly deduces the internal energy dissipation power equations and various external forces power equations of the 3D retaining wall under the nonlinear strength condition, such as to establish the work-energy balance equation. The pseudo-static method is used to consider the effect of earthquake on active earth pressure in horizontal state. The failure mode is a 3D curvilinear cone failure mechanism. For the different width of the retaining wall, the plane strain block is inserted in the symmetric plane. By optimizing all parameters, the maximum value of active earth pressure is calculated. In order to verify the validity of the new expressions obtained by the paper, the solutions are compared with previously published solutions. Agreement shows that the new expressions are effective. The results of different parameters are given in the forms of figures to analysis the influence caused by nonlinear strength parameters.

Keywords: limit analysis; nonlinear yield criterion; 3D active earth pressure; earthquakes

1. Introduction

The active earth pressure behind retaining wall is a classical and important theme in geotechnical engineering (Jo *et al.* 2017, Li and Yang 2018c, 2019c, Liu *et al.* 2009, Pain *et al.* 2017, Rao *et al.* 2016, Santos and Barros 2015, Yang and Zhang 2019, Zheng *et al.* 2015). In the previous literatures, the main methods can be divided into the following three categories: (a) the limit analysis method, (b) the limit equilibrium method, and (c) the numerical approaches. The numerical methods, including discrete element method and finite element method, can solve the problem more accurately than limit equilibrium method (Ugai and Leshchinsky 1995). However, the process of calculating three-dimensional (3D) active earth pressure by numerical method is very time-consuming. And it is difficult to model and verify the results. The traditional limit equilibrium method is still the most usually method in the calculation of active earth pressure. Pain *et al.* (2015) used the limit equilibrium method to analyze a gravity retaining wall supporting cohesionless backfill by modified pseudo-dynamic seismic forces. Pain *et al.* (2017) used the limit equilibrium method to make rotational stability analysis of gravity retaining wall on rigid foundation supporting dry cohesionless backfill with modified pseudo-dynamic seismic forces. Unfortunately, most of the limit equilibrium methods contain some unprovable assumptions relating to the internal to meet relevant requirements. The upper bound limit analysis shows superiority by comparing these three methods. It can be solved by work-energy

balance equation when only one unknown is involved. In the past, the most research of active earth pressure was generally focused on the two-dimensional plane strain. As a matter of fact, in many geotechnical engineering, the active pressure often becomes more of a 3D problem. Furthermore, the earthquake has considerable influence on the calculation of active earth pressure (Nian *et al.* 2014). Many researchers (Saran and Gupta 2003 and Shukla *et al.* 2009) have improved this work to account for $c-\phi$ backfills. Pain *et al.* (2018) proposed an analytical model for the evaluation of seismic active thrust on retaining wall. Rajesh and Choudhury (2016) proposed closed-form generalized solutions for computing seismic active earth thrust. To obtain a more realistic solution, it is necessary to propose a method to calculate the seismic active earth pressure correctly under the 3D condition.

According to many experiments, the failure envelopes of soil show the significant nonlinear characteristics. Triaxial tests show that there is a nonlinear relationship among the main stresses during the failure process of soil. The friction angle increases with the increase of compressive stress. Linear Mohr-Coulomb strength criterion underestimates the internal friction angle of soil while overestimating the large principal stress value of material failure. Zhang and Chen (1987) did research on the stability of two-dimensional slopes under nonlinear strength condition. Gao *et al.* (2015) calculated the critical heights of uniform slopes to explore the influence of nonlinear failure criterion on the slope stability. At present, most of the calculations of active earth pressure in the previous literatures were based on the linear strength condition. According to the aforementioned research results, there is a significant shortage in the study of the active earth pressure, especially the 3D active earth pressure under the nonlinear strength condition.

*Corresponding author, Professor
E-mail: csuyang@aliyun.com

This paper investigates the static and seismic active earth pressure of retaining wall under 3D condition and the soil obeys the nonlinear failure criterion. The method can be used to calculate both static and seismic active earth pressure on the non-vertical walls or vertical walls. Earthquake effects is solved by the *MO* model, which considered the horizontal seismic coefficient as a constant. Based on the 3D rotational failure mechanism under nonlinear strength condition, the dissipation rate of various external forces and internal energy is derived by using the principle of virtual work. Coding the corresponding computer program, the results of 3D active earth pressure under nonlinear strength condition can be obtained. The final results are compared with the present solutions which are obtained under the nonlinear or linear strength condition to verify the validity of this method. The comparisons prove that this method provides an efficient approach for calculating the 3D static and seismic active earth pressure under nonlinear strength condition. Based on the strength characteristics of the soil, the results of seismic active earth pressure under linear and nonlinear failure criteria are compared. This method is also used to study the influence caused by various parameters in the nonlinear yield criterion.

2. Upper bound theorem of limit analysis

Recently, limit analysis method has been widely used in geomechanics and engineering (Li and Yang 2018a, b, 2019a, b, Luo and Yang 2018). In the kinematic upper bound theorem, the soil mass abides by the associated rules and the soil obeys the convex yield function. There is a condition must be met that the work rate caused by external forces is not greater than the energy dissipation rate. This can be presented by the following equation

$$\int_V \sigma_{ij} \dot{\epsilon}_{ij} dV \geq \int_S T_i v_i dS + \int_V X_i v_i dV \quad (1)$$

where σ_{ij} and $\dot{\epsilon}_{ij}$ are the stress rate tensor and strain rate tensor respectively; V and S are the volume and the boundary of the collapse block respectively; T_i refers to surcharge load on boundary; X_i denotes the body force in V ; v_i refers to the velocity along the sliding surface.

3. Nonlinear Mohr-Coulomb yield criterion

A lot of experiments have proved that the linear strength criterion cannot describe the failure envelope of soils in τ - σ_n stress space accurately (Xu *et al.* 2018, Xu and Yang 2019, Zou and Xia 2016). To solve this problem, Zhang and Chen (1987) presented the nonlinear failure criterion of cohesive soils. In recent years, the nonlinear strength criterion has been widely used in many aspects. The criterion in τ - σ_n stress space is expressed as

$$\tau = c_0 \left(1 + \frac{\sigma_n}{\sigma_t} \right)^{\frac{1}{m}} \quad (2)$$

where σ_n and τ are the normal stress and shear stress of the failure envelope (or surface), respectively. Where c_0 ($c_0 \geq 0$) is the initial cohesion of soil at zero stress, σ_t ($\sigma_t \geq 0$) is the

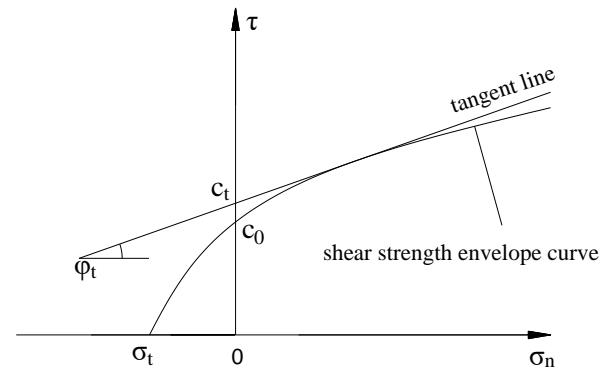


Fig. 1 Nonlinear failure criterion and generalized tangent line

absolute value of tensile stress when τ is equal to zero, and m ($m \geq 0$) is used to control the curvature of nonlinear failure envelope. When $m=1$, the nonlinear failure envelope overlaps with the linear strength criterion envelope. The specific value of c_0 , σ_t and m can be obtained by experiments. In order to apply the nonlinear strength criterion to the calculation of the main power of 3D retaining wall, the generalized tangent technique is introduced to obtain the equivalent strength parameters under the nonlinear strength criterion. The method uses a tangent line outside the envelope of nonlinear strength to obtain the related strength parameters. As show in Fig. 1, the equation of the external tangent is

$$\tau = c_t + \sigma_n \tan \varphi_t \quad (3)$$

where $\tan \varphi_t$ and c_t are the slope and vertical intercept of the tangent line, respectively. The $\tan \varphi_t$ represents the tangent value of the equivalent angle of internal friction of soil. The c_t represents the equivalent cohesive force of soil. A independent variable φ_t ($0 < \varphi_t < \pi/2$) is introduced as $\tan \varphi_t = d\tau/d\sigma_n$. Using Eq. (2) and Eq. (3), the soil cohesive force is expressed as

$$c_t = \tau - \sigma_n \tan \varphi_t = \frac{m-1}{m} c_0 \left(\frac{m\sigma_t \tan \varphi_t}{c_0} \right)^{\frac{1}{1-m}} + \sigma_t \tan \varphi_t \quad (4)$$

4. Calculation of 3D active earth pressure

4.1 Rotational failure mechanism

In the 3D failure mechanism, the discontinuity of velocity is required to be tangent to the cone with an apex Angle of $2\varphi_t$, and the axis of the cone coincides with the linear velocity v of soil rotation. Michalowski and Drescher (2009) proposed the destruction mechanism of the curved cone, and the mechanism has been widely employed in stability analysis (Yang and Chen 2019, Yang and Liu 2018, Yang and Li 2018, Zhu and Yang 2018). The mechanism is shown diagrammatically is Fig. 2.

Under the nonlinear condition of soil strength, the failure mechanism of 3D retaining wall is composed of a varying circle rotation defined by two log-spirals. The

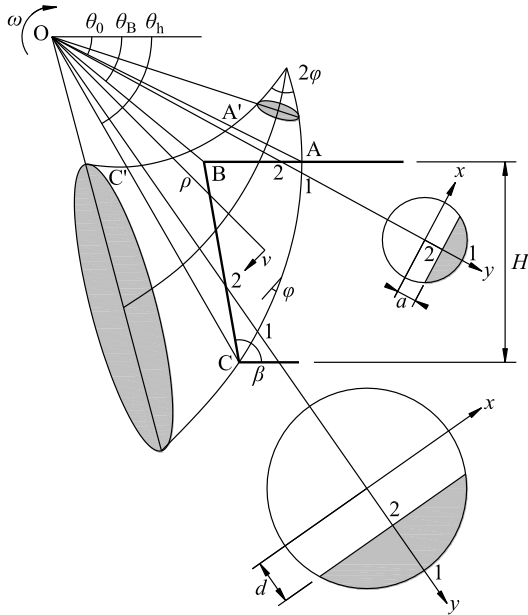


Fig. 2 3D rotational failure mechanism for the retaining wall

with $r_0=OA$, $r'_0=OA'$, and θ_0 shown in Fig. 2. When the parameters of 3D retaining wall and the type of soils are known, the failure mechanism is completely determined by three variables which are the ratio r'_0/r_0 , the angle θ_h and the angle θ_0 . According to the failure mode in Fig. 2, the distance from the center of rotation O to the center of the section of any rotation radius r_m and the radius R of any circular section are respectively expressed as

$$r_m = (r + r')/2 = r_0 f_1 \tag{7}$$

$$R = (r - r')/2 = r_0 f_2 \tag{8}$$

where f_1 and f_2 are two dimensionless functions given in Appendix.

In the calculation, the width of the 3D retaining wall cannot be ignored. In the failure mechanism shown in Fig. 3, a plane strain block with width b is inserted into the symmetric plane. The inserted width b can be obtained as follows

$$b = B - B'_{max} \tag{9}$$

In this way, the width of 3D retaining wall will no longer be limited at calculation time. This is obvious that it will be converted to plane strain problem when the inserted width $b \rightarrow \infty$. The inserted block divides the failure mechanism shown in Fig. 3 into two parts on average. Both the two parts have the same geometric shape as log-spiral AC.

4.2 Power balance equation

When solving the active earth pressure problem through limit analysis, it is necessary to calculate the internal energy dissipation rate and various external work rate of the 3D retaining wall failure mechanism shown in Fig. 2. All external power is provided by soil gravity, retaining wall adhesion, active earth pressure and seismic inertia force. The force diagram is illustrated in Fig. 4.

The internal energy dissipation rate occurred on the potential sliding surface AC in the failure mechanism of retaining wall. According to the failure mechanism shown in the diagram, each work rate can be divided into two parts: the 3D part and the plane strain block part. When calculating the power of the 3D part, as shown in Fig. 2, a local Cartesian coordinate system is established in the

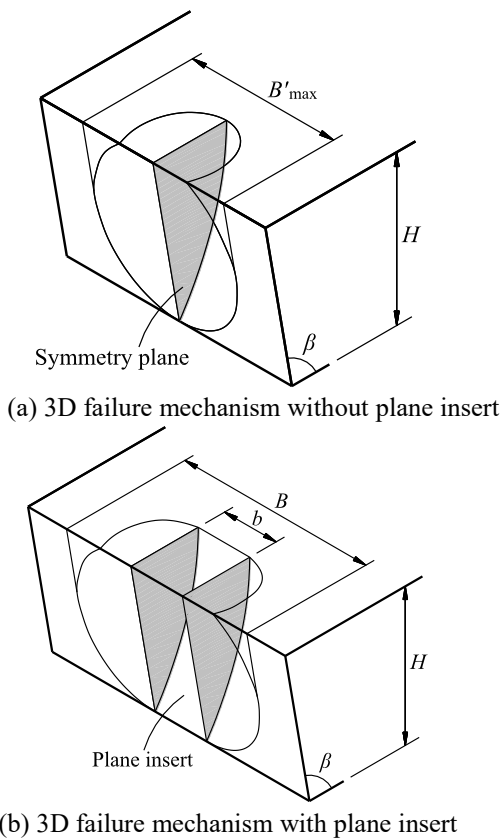


Fig. 3 Schematic diagram of the 3D failure mechanism

destruction mechanism consists of two log-spirals, respectively are AC and A'C'

$$AC = r = r_0 e^{(\theta - \theta_0) \tan \varphi} \tag{5}$$

$$A'C' = r' = r'_0 e^{-(\theta - \theta_0) \tan \varphi} \tag{6}$$

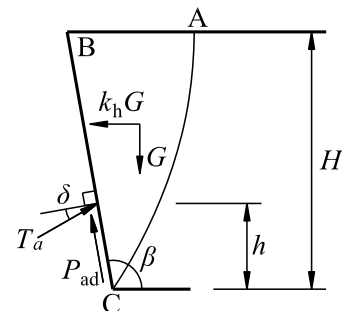


Fig. 4 Force diagram of the retaining wall

circular section of the plane perpendicular to any x-axis in the range $(\theta_B - \theta_0)$ and $(\theta_h - \theta_B)$, where θ_B can be deduced from geometric relations and expressed as

$$\theta_B = \arctan \frac{\sin \theta_0}{\cos \theta_0 - \kappa_2} \quad (10)$$

where κ_2 is a function about φ_t which is given in Appendix. The expressions of double or triple integrals are obtained by calculation. The plane strain block part can be directly obtained by the product of strain block width b and two-dimensional plane strain, which has been obtained in previous papers. Therefore, the work rate of the strain block part is not derived in detail. If the angular velocity of the entire failure mechanism around the axis O is ω , the linear velocity (v) at any position is expressed as

$$v = (r_m + y)\omega \quad (11)$$

The internal energy dissipation rate on the potential sliding surface AC can be obtained by the following formula

$$\dot{W}_{\text{int}} = \int_{S_t} c_t v \cos \varphi_t dS_t \quad (12)$$

where \dot{W}_{int} is the work rate of internal energy dissipation, S_t is the area of the sliding surface and c_t is the soil cohesive force corresponding to different φ_t under nonlinear conditions, and its value can be obtained by Eq. (4). Using geometrical relations, the energy dissipation rate of soil in the 3D part of retaining wall is

$$\dot{W}_{\text{int-3D}} = 2\omega c_t \left[\int_{\theta_0}^{\theta_b} \int_a^R \frac{R(r_m + y)^2}{\sqrt{R^2 - y^2}} dy d\theta + \int_{\theta_b}^{\theta_h} \int_d^R \frac{R(r_m + y)^2}{\sqrt{R^2 - y^2}} dy d\theta \right] \quad (13)$$

where $\dot{W}_{\text{int-3D}}$ is the internal energy dissipation rate of the 3D part, R and r_m have been given in this paper, a and b can be expressed as follows

$$a = \frac{\sin \theta_0}{\sin \theta} r_0 - r_m = r_0 f_3 \quad (14)$$

$$d = \frac{\sin(\beta + \theta_h)}{\sin(\beta + \theta)} r_0 e^{(\theta_h - \theta) \tan \varphi_t} - r_m = r_0 f_4 \quad (15)$$

where β is the inclined angle of retaining wall, f_3 and f_4 are two functions given in Appendix. Hence, for the sake of convenient in recording, the internal energy dissipation rate of 3D part $\dot{W}_{\text{int-3D}}$ is

$$\dot{W}_{\text{int-3D}} = \omega c_t r_0^3 g_1 \quad (16)$$

with g_1 is a function given in Appendix. With the help of previous papers, the energy dissipation rate $\dot{W}_{\text{int-insert}}$ of the plane strain block part is expressed as

$$\dot{W}_{\text{int-insert}} = \omega c_t r_0^3 g_2 \quad (17)$$

in which g_2 being a function given in Appendix.

The gravity work rate of soil of any unit volume in the

retaining wall can be expressed as

$$d\dot{w} = \gamma v \cos \theta dV = \gamma v \cos \theta dx dy (r_m + y) d\theta \quad (18)$$

where γ is the unit weight of soil masses. From the Eq. (18), the work rate caused by gravity $\dot{W}_{\gamma-3D}$ of 3D part of soil can be expressed as

$$\dot{W}_{\gamma-3D} = 2\omega \gamma \left[\int_{\theta_0}^{\theta_b} \int_a^R \int_0^{\sqrt{R^2 - y^2}} (r_m + y)^2 \cos \theta dx dy d\theta + \int_{\theta_b}^{\theta_h} \int_d^R \int_0^{\sqrt{R^2 - y^2}} (r_m + y)^2 \cos \theta dx dy d\theta \right] \quad (19)$$

Earthquake usually has two effects on the retaining wall. On the one hand it increases the driving force of retaining wall, on the other hand it can decrease the shear strength of soil. In many cases, the effect of the earthquake on the retaining wall is reflected in the increase of the driving force. Only when the earthquake magnitude reaches a certain limit or the actual situation and conditions of the ground are favorable for the reduction of shear strength of soil can the effect of the reduction of shear strength of soil be reflected. Therefore, in this paper, as many researchers do, the effect of earthquake on retaining wall is only considered to increase the driving force. According to the *MO* model, the horizontal seismic coefficient in this paper is a constant. The value of the horizontal seismic coefficient k_h ranges from (0.0-0.2). Therefore, the calculation method of seismic inertia force work rate about the 3D part is similar to the gravity work rate calculation of soil. The work rate of seismic force \dot{W}_{k_h-3D} of the 3D part is expressed as

$$\dot{W}_{k_h-3D} = 2\omega \gamma k_h \left[\int_{\theta_0}^{\theta_b} \int_a^R \int_0^{\sqrt{R^2 - y^2}} (r_m + y)^2 \sin \theta dx dy d\theta + \int_{\theta_b}^{\theta_h} \int_d^R \int_0^{\sqrt{R^2 - y^2}} (r_m + y)^2 \sin \theta dx dy d\theta \right] \quad (20)$$

The value of tangential action intensity adhesive force P_{ad} is $c_t \tan \delta / \tan \varphi_t$ per unit area, where δ is the soil-wall friction angle. The work rate caused by the adhesive force of 3D part is expressed as

$$\dot{W}_{P_{ad}-3D} = 2\omega c_t r_0^2 \frac{\tan \delta \sin^2(\theta_h + \beta)}{\tan \varphi_t} e^{2(\theta_h - \theta) \tan \varphi_t} \int_{\theta_0}^{\theta_b} \int_0^{\sqrt{R^2 - d^2}} \frac{dx d\theta}{\sin^2(\theta + \beta)} \quad (21)$$

Similarly, the work rate caused by soli weight ($\dot{W}_{\gamma-insert}$), seismic inertia force ($\dot{W}_{k_h-insert}$) and intensity adhesive force ($\dot{W}_{P_{ad}-insert}$) of the plane strain block part can be written as

$$\begin{cases} \dot{W}_{\gamma-insert} = \omega \gamma r_0^4 g_4 \\ \dot{W}_{k_h-insert} = \omega \gamma k_h r_0^4 g_6 \\ \dot{W}_{P_{ad}-insert} = \omega c_t r_0^3 g_8 \end{cases} \quad (22)$$

where g_4 , g_6 , and g_8 are three functions given in Appendix.

As the same with most scholars, when calculating the work rate of active earth pressure, the position of the operating point is assumed to be at lower 1/3 of the retaining wall height. Therefore, the work rate of the active earth pressure P_{ae} can be expressed as

$$\dot{W}_{P_{ae}} = \omega r_0 P_{ae} g_9 \quad (23)$$

where g_9 is a function given in Appendix. For convenience of recording, the Eq. (19)-(21) are rewritten as

$$\begin{cases} \dot{W}_{\gamma-3D} = \omega \gamma r_0^4 g_3 \\ \dot{W}_{k_h-3D} = \omega \gamma k_h r_0^4 g_5 \\ \dot{W}_{P_{ad}-3D} = \omega c_t r_0^3 g_7 \end{cases} \quad (24)$$

where g_3 , g_5 , and g_7 are three functions given in Appendix.

According to the aforementioned analysis, the work rate balance equation based on upper bound limit analysis method under the condition of nonlinear strength can be written as

$$\dot{W}_{int} + \dot{W}_{P_{ae}} + \dot{W}_{P_{ad}} = \dot{W}_{\gamma} + \dot{W}_{k_h} \quad (25)$$

where \dot{W}_{int} is the rate of internal energy dissipation, $\dot{W}_{P_{ae}}$ is the work rate caused by the total force of active earth pressure, $\dot{W}_{P_{ad}}$ is the work rate caused by the adhesive, \dot{W}_{γ} is the work rate caused by the soil weight, and \dot{W}_{k_h} is the work rate caused by the seismic force. All of them are the sum of their 3D part and the plane strain block part which have been calculated in this paper. Notice that the left of the equation Eq. (25) means that the forces do negative work.

4.3 Active earth pressure calculation

Substituting corresponding equations into Eq. (25) and after rearranging it, the expression of the earth active pressure P_{ae} can be obtained. P_{ae} is a complex quantity about functions g_1 – g_9 which have been mentioned in this paper. It can be expressed as

$$P_{ae} = \frac{\gamma r_0^3 (g_3 + g_4) + \gamma k_h r_0^3 (g_5 + g_6) - c_t r_0^2 (g_1 + g_2 + g_7 + g_8)}{g_9} \quad (26)$$

Like most scholars, the force of per unit width is generally considered when analyzing of active earth pressure. Therefore, the equivalent width B_e is introduced to estimate the thrust of seismic active earth pressure p_{ae} . In the calculation of the active earth pressure of 3D retaining wall, it is assumed that the area of failure surface is equal to the area of equivalent width of retaining wall, and the equivalent width B can be obtained by calculating the area of failure surface of retaining wall. As shown in Fig. 3, it can be seen that $b > B_e < B$, and B_e is the most appropriate to be the equivalent width to estimate in the three quantities. It can be estimated by

$$B_e = \frac{A}{H/\sin \beta} \quad (27)$$

where A is the area of failure surface on the soil-wall interface. The area A can also be divided into 3D part and plane strain block part. The area A can be calculated by

$$A = 2r_0 e^{(\theta_h - \theta_0) \tan \varphi_i} \sin(\theta_h + \beta) \int_{\theta_b}^{\theta_h} \int_0^{\sqrt{R^2 - d^2}} \frac{dx d\theta}{\sin^2(\theta + \beta)} + \frac{bH}{\sin \beta} \quad (28)$$

By plugging area A into the Eq. (27), the equivalent width B_e can be written as

$$B_e = r_0 g_{10} \quad (29)$$

where g_{10} is a function that has been reported in Appendix. Hence, the thrust of seismic active earth pressure p_{ae} can be defined as the ratio of P_{ae} to B_e , and it can be expressed as

$$p_{ae} = P_{ae} / B_e \quad (30)$$

Substituting corresponding equations into Eq. (30) and after rearranging it, the expression of the thrust of seismic earth active pressure p_{ae} can be rewritten as

$$p_{ae} = \frac{\gamma r_0^2 (g_3 + g_4) + \gamma k_h r_0^2 (g_5 + g_6) - c_t r_0 (g_1 + g_2 + g_7 + g_8)}{g_9 g_{10}} \quad (31)$$

For more convenient application, the thrust p_{ae} can be expressed as

$$p_{ae} = \frac{1}{2} \gamma H^2 K_{ae} \quad (32)$$

where K_{ae} is a coefficient about the active earth pressure. It can be determined by some parameters, which are the inclined angle β , the seismic coefficient K_h , the ratio B/H , the soil gravity γ , the soil-wall friction angle δ , the soil cohesion c_t , and the nonlinear coefficient m . In order to ensure that the mechanism of failure is valid in the subsequent parameter optimization analysis, the following geometric constraints need to be added

$$\begin{cases} 0 < \theta_0 < \theta_B < \theta_h < \pi \\ 0 < r'_0 / r_0 < 1 \\ 0 < \varphi_t < \pi / 2 \\ b \geq 0 \\ |a| < R \\ |d| < R \end{cases} \quad (33)$$

where $||$ is the absolute value sign. In the process of the failure mechanism, there is a nonlinear relationship between each principal stress, and the friction angle φ_t is increased with the increase of the compressive stress. Therefore, the third constraint is established to meet the nonlinear condition of soil strength. To make sure that the trace $A'C'$ will not get across the retaining wall in the failure mechanism, the fifth and the sixth constraints are made. After giving other soil parameters and retaining wall parameters, four parameters the ratio r'_0 / r_0 , the angle θ_h , the angle θ_0 and the friction angle φ_t in Eq. (32) are optimized and analyzed by the sequential quadratic programming to obtain the maximum value among all of the results. The initial value of this programming can be obtained by the method of exhaustion. The dichotomy is used to obtain the rough value. And then, the final result is obtained by SQP algorithm. The constraints of the SQP algorithm have been listed above in this paper.

5. Comparisons

5.1 Comparison of results under nonlinear criterion

In the previous research, a literature of Gao *et al.* (2015)

Table 1 More accurate results than Gao *et al.* (2015) for London clay

$\beta=90^\circ; k_h=0.0$	B/H				
	1	2	5	10	∞
Corresponding critical heights of Gao <i>et al.</i> (m)	2.318	1.809	1.605	1.557	1.497
Present solutions	1.208	0.228	0.059	0.040	0.002

Table 2 Comparisons between the present solutions with Antão *et al.* (2015) corresponding to $k_h=0.0, \beta=90^\circ$

B/H	φ	δ/φ (Results of this paper)					δ/φ (Results of Antão <i>et al.</i> 2015)				
		0	1/3	1/2	2/3	1	0	1/3	1/2	2/3	1
		1.0	15°	0.498	0.469	0.457	0.447	0.434	0.524	0.493	0.482
	20°	0.393	0.365	0.355	0.3488	0.341	0.423	0.393	0.383	0.377	0.371
	25°	0.307	0.285	0.278	0.273	0.270	0.340	0.313	0.306	0.301	0.299
	30°	0.240	0.222	0.2175	0.215	0.215	0.271	0.250	0.244	0.241	0.244
	35°	0.188	0.173	0.169	0.168	0.172	0.214	0.198	0.194	0.193	0.200
	40°	0.146	0.135	0.133	0.133	0.139	0.164	0.156	0.154	0.154	0.164
	45°	0.112	0.104	0.103	0.104	0.113	0.132	0.122	0.121	0.123	0.135
	15°	0.540	0.510	0.501	0.494	0.483	0.560	0.524	0.513	0.505	0.497
	20°	0.436	0.411	0.402	0.397	0.390	0.455	0.425	0.415	0.408	0.404
	25°	0.351	0.328	0.322	0.318	0.317	0.371	0.350	0.336	0.340	0.331
2.0	30°	0.283	0.263	0.258	0.256	0.259	0.300	0.278	0.272	0.269	0.273
	35°	0.227	0.211	0.207	0.207	0.214	0.240	0.223	0.220	0.219	0.227
	40°	0.180	0.168	0.166	0.167	0.177	0.188	0.178	0.176	0.177	0.189
	45°	0.141	0.132	0.132	0.134	0.147	0.150	0.140	0.140	0.142	0.158
	15°	0.564	0.536	0.527	0.520	0.508	0.575	0.543	0.532	0.524	0.516
	20°	0.464	0.437	0.428	0.422	0.417	0.475	0.445	0.435	0.428	0.424
	25°	0.381	0.356	0.349	0.344	0.344	0.390	0.363	0.355	0.350	0.351
5.0	30°	0.311	0.290	0.284	0.282	0.286	0.319	0.296	0.290	0.287	0.293
	35°	0.252	0.234	0.231	0.231	0.239	0.257	0.239	0.235	0.235	0.245
	40°	0.201	0.188	0.186	0.188	0.200	0.204	0.192	0.190	0.191	0.205
	45°	0.158	0.148	0.148	0.151	0.168	0.161	0.151	0.147	0.15	0.172
	15°	0.588	0.556	0.545	0.537	0.526	0.588	0.556	0.546	0.537	0.530
	20°	0.490	0.459	0.449	0.441	0.435	0.489	0.458	0.449	0.442	0.438
	25°	0.405	0.377	0.369	0.364	0.362	0.404	0.377	0.369	0.364	0.365
∞	30°	0.333	0.309	0.303	0.300	0.304	0.331	0.308	0.302	0.300	0.306
	35°	0.271	0.251	0.247	0.246	0.255	0.269	0.250	0.246	0.246	0.257
	40°	0.217	0.202	0.200	0.201	0.215	0.214	0.200	0.198	0.200	0.215
	45°	0.171	0.160	0.160	0.163	0.181	0.168	0.158	0.158	0.161	0.180

gave the critical height of slope failure when the inclined angle $\beta=90^\circ$ under the condition of nonlinear strength failure criterion. As we know, when the height of retaining wall is critical, the value of active earth pressure should be zero. In this way, we can substitute the critical height H of retaining wall into the formulas. The active earth pressure is zero to determine whether the result is correct. This critical height is used to calculate the active earth pressure of London soil under different B/H conditions. The results are

shown in the Table 1. It can be seen from Table 1 that the results of this paper are close to the results of Gao *et al.* (2015). The active soil pressure coefficient is very close to zero, and its value is closer to zero with the increase of the ratio of width to height. The comparison shows that the present method is effective.

5.2 Comparison of results under linear criterion

It is seen from the previous discussion that when the nonlinear coefficient $m=1$, the nonlinear problem in this paper can be transformed into a linear problem. Based on the linear Mohr-Coulomb failure criterion, Antao *et al.* (2015) use the 3D implementation to determine the horizontal active earth pressure coefficients K_{ah} under static condition. And under the same conditions with Antao *et al.* (2015), we can verify the validity of the proposed method. Theoretically, the same results as Antao *et al.* (2015) can be obtained without considering the earthquake effects and the retaining wall is vertical when given the values of specific parameters C, φ, σ and δ . The data for comparison is shown in the Table 2. It can be seen that the results obtained by the two methods are only slightly different. The slight difference in the results may be due to the different failure mechanism and calculation methods of the two methods. Therefore, by comparing with the existing results of 3D active soil pressure under the linear yield criterion, it can be seen that this method of this paper is an effective method to evaluate active soil pressure.

6. Charts and parameter analysis

6.1 Results and discussions

When the inserted block is infinite in the 3D failure mode, the failure mode is close to the plane strain problem. That is, when the ratio of width to height B/H of 3D retaining wall is large enough, the 3D retaining wall degrades into a two-dimensional plane strain. Therefore, the value of variable B/H is intended to be the x-coordinate varying from 0 to 10 to reflect the variation of the active earth pressure coefficient from the 3D active earth pressure to the two-dimensional case.

The linear and nonlinear parameters shown in Table 3 of four kinds soils is found by the literature presented by Gao *et al.* (2015). Figs. 5 and 6 illustrate the effects of the inclined angle of the wall β and the seismic coefficient k_h on earth pressure coefficient about London clay and Upper Lias clay.

Table 3 Linear and nonlinear strength parameters for various soils

Soils	$\gamma(\text{kN/m}^3)$	Linear parameters			Nonlinear parameters	
		$c(\text{kPa})$	$\phi(^{\circ})$	$C_0(\text{kPa})$	$\sigma_s(\text{kPa})$	m
Israeli clay	18.0	11.7	24.7	0.06	0.02	1.23
London clay	18.0	6.0	32.0	1.07	0.15	1.66
Upper Lias clay	20.0	17.0	23.0	0.98	0.33	1.38
Oxford clay	20.0	6.0	29.0	0.16	0.007	1.65

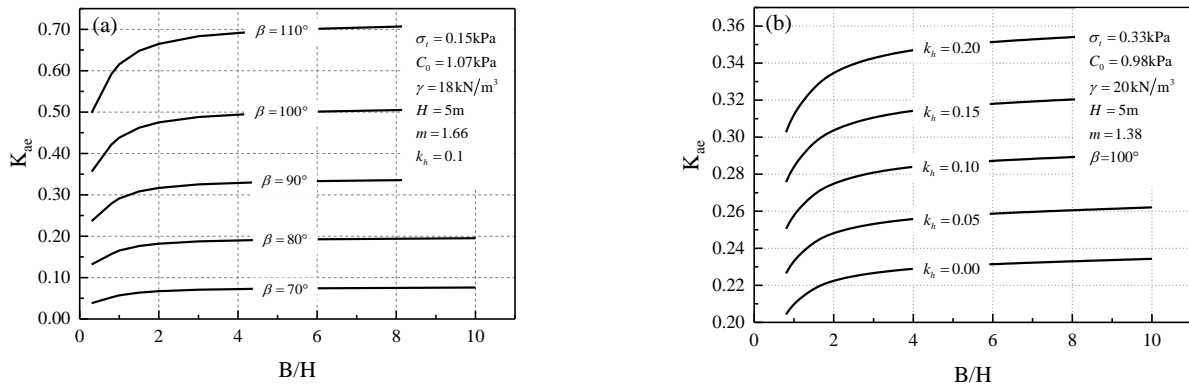


Fig. 5 Effects of parameters for Israeli clay: (a) inclined angle β and (b) seismic coefficient k_h

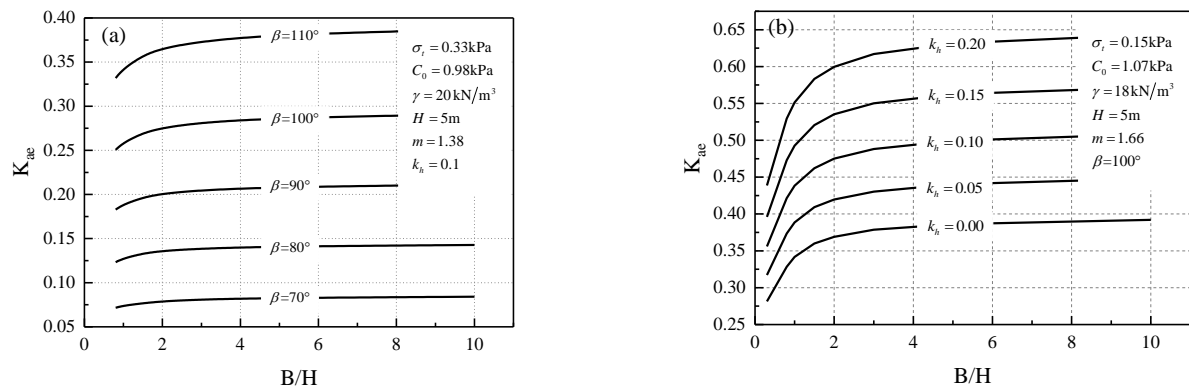


Fig. 6 Effects of parameters for Upper Lias clay: (a) inclined angle β and (b) seismic coefficient k_h

Table 4 Comparisons between the linear results with the nonlinear results (active earth pressure coefficients), corresponding to $k_h=0.0$ and $H=5 \text{ m}$

B/H	Results	ϕ (Israeli clay)				
		70°	80°	90°	100°	110°
2	Linear criterion	-0.0263	0.0508	0.1321	0.2224	0.3252
	Nonlinear criterion	0.1379	0.1918	0.2528	0.3260	0.4118
5	Linear criterion	-0.0187	0.0596	0.1429	0.2367	0.3451
	Nonlinear criterion	0.1416	0.1968	0.2607	0.3356	0.4271
10	Linear criterion	-0.016	0.0625	0.1465	0.2420	0.3525
	Nonlinear criterion	0.1428	0.1985	0.2637	0.3423	0.4329
B/H	Results	ϕ (London clay)				
		70°	80°	90°	100°	110°
2	Linear criterion	0.0756	0.1368	0.2047	0.2824	0.3750
	Nonlinear criterion	0.0337	0.0911	0.1584	0.2376	0.3325
5	Linear criterion	0.0804	0.1427	0.2132	0.2945	0.3916
	Nonlinear criterion	0.0369	0.0960	0.1661	0.2497	0.3494
10	Linear criterion	0.0820	0.1447	0.2160	0.2992	0.3979
	Nonlinear criterion	0.0380	0.0976	0.1688	0.2542	0.3559
B/H	Results	ϕ (Upper Lias clay)				
		70°	80°	90°	100°	110°
2	Linear criterion	-0.1296	-0.0427	0.0469	0.1451	0.2555
	Nonlinear criterion	0.0790	0.1360	0.2008	0.2755	0.3656
5	Linear criterion	-0.1214	-0.0324	0.0590	0.1609	0.2760
	Nonlinear criterion	0.0828	0.1411	0.2084	0.2867	0.3814

Table 4 Continued

B/H	Results	φ (Upper Lias clay)				
		70°	80°	90°	100°	110°
10	Linear criterion	-0.1186	-0.02892	0.0629	0.1662	0.2841
	Nonlinear criterion	0.0841	0.1428	0.2111	0.2910	0.3870
B/H	Results	φ (Oxford clay)				
		70°	80°	90°	100°	110°
2	Linear criterion	0.1241	0.1852	0.2530	0.3302	0.4230
	Nonlinear criterion	0.0596	0.1179	0.1879	0.2685	0.3635
5	Linear criterion	0.1296	0.1919	0.2622	0.3429	0.4402
	Nonlinear criterion	0.0635	0.1230	0.1966	0.2363	0.2806
10	Linear criterion	0.1314	0.1941	0.2655	0.3472	0.4469
	Nonlinear criterion	0.0647	0.1253	0.1996	0.2857	0.3874

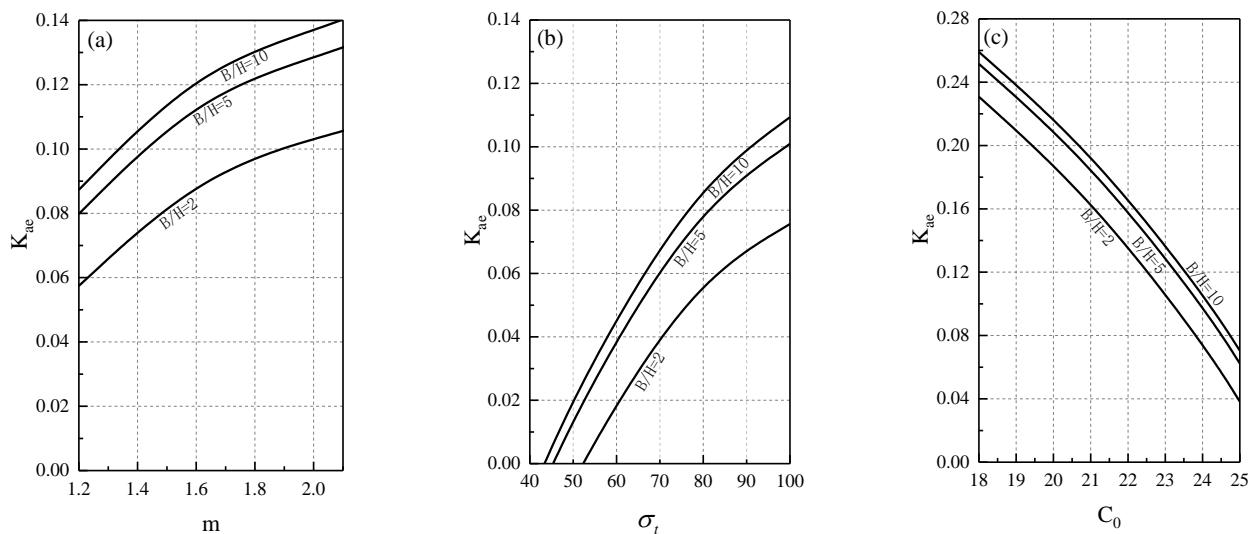


Fig. 7 Effects of nonlinear strength parameters: (a) nonlinear coefficient m , (b) tensile stress σ_t (kPa) and (c) initial cohesive force C_0 (kPa)

From the results as shown in Fig. 5, it can be found that when the ratio B/H is small, the impact of the 3D effect is greater. The coefficient of the active earth pressure tends to a constant value and it almost has no difference from two-dimensional retaining wall when the ratio is great enough. That is, when the ratio B/H is smaller than 10.0, with an eye to the 3D effect is necessary. From the Figs. 5 and 6, both the London clay and the Upper Lias clay embody the same trends. It is obvious that the results increase with the increasing of the inclined angle β and the seismic coefficient k_h . Furthermore, for different soils, the corresponding earth active pressure coefficients have different sensitivity to parameter variations. The effects of the k_h for Upper Lias clay is less obvious when the ratio B/H is smaller than that for Israeli clay. This rule is not suitable for the β , when the B/H is small the results are not change a lot, just embodying a bit of trends. It is guessed that the seismic coefficient k_h has more influence on the 3D failure mechanism than the inclined angle β .

In order to compare the effect of nonlinear and linear failure criterion on the active earth pressure coefficient of 3D retaining wall, all kinds of soils showed in Table 3

are used in this paper. Table 4 list the two different criterions results of all soils corresponding to $H=5$ m, $k_h=0.1$ and $\delta=0^\circ$, with the fictional angle β varying from 70° to 110° , and the ratios B/H are 2, 5 and 10, respectively. The results are the same as the actual situation. There exists difference between the nonlinear case and the linear case. The values of nonlinear case can better reflect the real properties of soil.

6.2 Influences of the soil parameters

The soil parameters have significant effects on the active earth pressure coefficient of the 3D retaining wall, including nonlinear coefficient m (1.2~2.0), tensile stress σ_t (40~100) and initial cohesive force C_0 (18~25). The values of the active earth pressure coefficient corresponding to $\gamma=19.63$ kN/m³, $k_h=0.1$, $\beta=100^\circ$, $m=1.4$, $\sigma_t=89.35$ kPa, $C_0=23.94$ kPa and $H=5$ m, for the radio $B/H=2, 5$ and 10 are illustrated in Fig. 7.

It can be seen from Fig. 7 that the value of active earth pressure coefficient is increased with the increasing of m and σ_t . On the contrary, the rule shown by C_0 is that the

coefficient is decreased with the increasing of initial cohesive. The parameter analysis in the Fig. 7 shows that the nonlinearity of soil strength has significant influence on the active earth pressure coefficient of the retaining wall. For instance, when the nonlinear coefficient m increases from 1.2 to 2.0 and $B/H=2$, the value of active earth pressure coefficient increases from 0.057 to 0.104. An 82 percent increases from previous results indicates that the nonlinear soil strength is a nonnegligible factor that has a significant impact on the active earth pressure coefficient of retaining wall.

7. Conclusions

This paper develops new expressions to calculate 3D earth pressure, which incorporates the nonlinear Mohr-Coulomb yield criterion into the upper bound limit analysis of the seismic active earth pressure against retaining wall. The dissipation rate of various external forces and internal energy is derived by using the principle of virtual work. The computation results obtained by the optimization scheme in present study compared with those from nonlinear and linear solutions. Validity of the new expressions verified by those comparison results, which provides an efficient approach for calculating the 3D static and seismic active earth pressure under nonlinear strength condition. Some conclusions can be condensed in point form:

- The solutions of the 3D active earth pressure are highly depend on the retaining soil property and wall geometry. It is found that for the retaining wall with narrow width, the influence of nonlinear failure criterion on the stability evaluation of the retaining wall is more significant.

- The sensitivity analysis is conducted to analyze the effects of the nonlinear coefficient, the tensile stress and the initial cohesive force on the static and seismic active earth pressure under 3D condition.

- In addition, the value of 3D active earth pressure of the retaining wall under nonlinear condition is smaller than that of two-dimensional case. When the ratio B/H is small, the impact of the 3D effect is greater. The coefficient of the active earth pressure tends to a constant value and it is almost no difference from two-dimensional retaining wall when the ratio is great enough.

Acknowledgements

The preparation of the paper has received financial supports from Innovation Foundation for Postgraduate of Central South University, China (2018zzts185). The financial supports are greatly appreciated.

References

Aminpour, M.M., Maleki, M. and Ghanbari, A. (2017), "Investigation of the effect of surcharge on behavior of soil slopes", *Geomech. Eng.*, **13**(4), 653-669.
 Antão, A.N., Santana, T., da Silva, M.V. and Guerra, N.M. (2016), "3D active earth pressure coefficients by upper bound

numerical limit analysis", *Comput. Geotech.*, **79**, 96-104.
 Gao, Y.F., Wu, D. and Zhang, F. (2015), "Effects of nonlinear failure criterion on the 3D stability analysis of uniform slopes", *Eng. Geol.*, **198**, 87-93.
 Jo, S.B., Hu, J.G., Lee, J.S. and Kim, D.S. (2017), "Evaluation of the seismic earth pressure for inverted T-shape stiff retaining wall in cohesionless soils via dynamic centrifuge", *Soil Dyn. Earthq. Eng.*, **92**, 345-57.
 Li, T.Z. and Yang, X.L. (2018a), "Probabilistic stability analysis of subway tunnels combining multiple failure mechanisms and response surface method", *Int. J. Geomech.*, **18**(12), 04018167.
 Li, Y.X. and Yang, X.L. (2018b), "Three-dimensional seismic displacement analysis of rock slopes based on Hoek-Brown failure criterion", *KSCE J. Civ. Eng.*, **22**(11), 4334-4344.
 Li, Y.X. and Yang, X.L. (2019a), "Seismic displacement of 3D slope reinforced by piles with nonlinear failure criterion", *Int. J. Geomech.*, **19**(6), 04019042.
 Li, Y.X. and Yang, X.L. (2019b), "Soil-slope stability considering effect of soil-strength nonlinearity", *Int. J. Geomech.*, **19**(3), 04018201.
 Li, Z.W. and Yang, X.L. (2019c), "Kinematical analysis of active earth pressure considering tension crack, pore-water pressure and soil nonlinearity", *KSCE J. Civ. Eng.*, **23**(1), 56-62.
 Li, Z.W. and Yang, X.L. (2018c), "Active earth pressure for soils with tension cracks under steady unsaturated flow conditions", *Can. Geotech. J.*, **55**(12), 1850-1859.
 Liu, F.Q., Wang, J.H. and Zhang, L.L. (2009), "Axi-symmetric active earth pressure obtained by the slip line method with a general tangential stress coefficient", *Comput. Geotech.*, **36**, 352-358.
 Luo, W.J. and Yang, X.L. (2018), "3D stability of shallow cavity roof with arbitrary profile under influence of pore water pressure", *Geomech. Eng.*, **16**(6), 569-575.
 Michalowski, R.L. and Drescher, A. (2009), "3D stability of slopes and excavations", *Géotechnique*, **10**, 839-850.
 Nian, T.K., Liu, B., Han, J. and Huang, R.Q. (2014), "Effect of seismic acceleration directions on dynamic earth pressures in retaining structures", *Geomech. Eng.*, **7**(3), 263-277.
 Pain, A., Chen, Q.S., Nimbalkar, S. and Zhou, Y.T. (2017), "Evaluation of seismic passive earth pressure of inclined rigid retaining wall considering soil arching effect", *Soil Dyn. Earthq. Eng.*, **100**, 286-295.
 Pain, A., Choudhury, D. and Bhattacharyya, S.K. (2015), "Seismic stability of retaining wall-soil sliding interaction using modified pseudo-dynamic method", *Géotech. Lett.*, **5**(1), 56-61.
 Pain, A., Choudhury, D. and Bhattacharyya, S.K. (2017), "Seismic rotational stability of gravity retaining walls by modified pseudo-dynamic method", *Soil Dyn. Earthq. Eng.*, **94**, 244-253.
 Pain, A., Ramakrishna Annareddy, V.S. and Nimbalkar, S. (2018), "Seismic active thrust on rigid retaining wall using strain dependent dynamic properties" *Int. J. Geomech.*, **18**(12), 06018034.
 Rajesh, B.G. and Choudhury, D. (2016), "Generalized seismic active thrust on a retaining wall with submerged backfill using a modified pseudodynamic method", *Int. J. Geomech.*, **16**(3), 06016023.
 Rao, P.P., Chen, Q.S., Zhou, Y.T., Nimbalkar, S. and Chiaro, G. (2016), "Determination of active earth pressure on rigid retaining wall considering arching effect in cohesive backfill soil", *Int. J. Geomech.*, **16**(3), 04015082.
 Santos, P.J. and Barros, P.L. (2015), "Active earth pressure due to soil mass partially subjected to water seepage", *Can. Geotech. J.*, **52**(11), 1886-91.
 Saran, S. and Gupta, R.P. (2003), "Seismic earth pressures behinds retaining walls", *Ind. Geotech. J.*, **33**(3), 195-213.
 Shukla, S.J., Gupta, S.K. and Sivakugan, N. (2009), "Active earth pressure on retaining wall for $c-\phi$ soil backfill under seismic

- loading conditions”, *J. Geotech. Geoenviron. Eng.*, **235**(5), 590-596.
- Ugai, K. and Leshchinsky, D.O.V. (1995), “3D limit equilibrium and finite element analyses: a comparison of results”, *Soil Found.*, **35**(4), 1-7.
- Xu, J.S. and Yang, X.L. (2019), “Seismic stability of 3D soil slope reinforced by geosynthetic with nonlinear failure criterion”, *Soil Dyn. Earthq. Eng.*, **118**, 86-97.
- Xu, J.S., Li, Y.X. and Yang, X.L. (2018), “Seismic and static 3D stability of two-stage slope considering joined influences of nonlinearity and dilatancy”, *KSCE J. Civ. Eng.*, **22**(10), 3827-3836.
- Yang, X.L. and Chen, J.H. (2019), “Factor of safety of geosynthetic-reinforced slope in unsaturated soils”, *Int. J. Geomech.*, **19**(6), 04019041.
- Yang, X.L. and Li, Z.W. (2018), “Comparison of factors of safety using a 3D failure mechanism with kinematic approach”, *Int. J. Geomech.*, **18**(9), 04018107.
- Yang, X.L. and Liu, Z.A. (2018), “Reliability analysis of three-dimensional rock slope”, *Geomech. Eng.*, **15**(6), 1183-1191.
- Yang, X.L. and Zhang, S. (2019), “Seismic active earth pressure for soils with tension cracks”, *Int. J. Geomech.*, **19**(6), 06019009.
- Zhang, X.L. and Chen, W.F. (1987), “Stability analysis of slopes with general nonlinear failure criterion”, *Int. J. Numer. Anal. Meth. Geomech.*, **11**(1), 33-50.
- Zheng, D.F., Nian, T.K., Liu, B., Yin, P. and Song, L. (2015), “Coefficient charts for active earth pressure under combined loadings”, *Geomech. Eng.*, **8**(3), 461-476.
- Zhu, J.Q. and Yang, X.L. (2018), “Probabilistic stability analysis of rock slopes with cracks”, *Geomech. Eng.*, **16**(6), 655-667.
- Zou, J.F. and Xia, Z.Q. (2016), “Theoretical solutions for displacement and stress of a circular opening reinforced by grouted rock bolt”, *Geomech. Eng.*, **11**(3), 439-455.

Appendix

$$\kappa_1 = \frac{H}{r_0} = \sin \theta_h e^{(\theta_h - \theta_0) \tan \varphi_i} - \sin \theta_0$$

$$\kappa_2 = \frac{L}{r_0} = \frac{\sin(\theta_0 + \beta) - \sin(\theta_h + \beta) e^{(\theta_h - \theta_0) \tan \varphi_i}}{\sin \beta}$$

$$f_1 = \frac{1}{2} \left[e^{(\theta - \theta_0) \tan \varphi_i} + \frac{r'_0}{r_0} e^{-(\theta - \theta_0) \tan \varphi_i} \right]$$

$$f_2 = \frac{1}{2} \left[e^{(\theta - \theta_0) \tan \varphi_i} - \frac{r'_0}{r_0} e^{-(\theta - \theta_0) \tan \varphi_i} \right]$$

$$f_3 = \frac{\sin \theta_0}{\sin \theta} - f_1$$

$$f_4 = \frac{\sin(\theta_h + \beta)}{\sin(\theta + \beta)} e^{(\theta_h - \theta_0) \tan \varphi_i} - f_1$$

$$f_5 = \frac{1}{3(1 + 9 \tan^2 \varphi_i)} \left[(3 \tan \varphi_i \cos \theta_h + \sin \theta_h) e^{3(\theta_h - \theta_0) \tan \varphi_i} - 3 \tan \varphi_i \cos \theta_0 - \sin \theta_0 \right]$$

$$f_6 = \frac{1}{6} \kappa_2 (2 \cos \theta_0 - \kappa_2) \sin \theta_0$$

$$f_7 = \frac{1}{6} \kappa_1 \frac{\sin(\theta_h + \beta)}{\sin \beta} e^{(\theta_h - \theta_0) \tan \varphi_i} \left[\cos \theta_0 - \kappa_2 + \cos \theta_h e^{(\theta_h - \theta_0) \tan \varphi_i} \right]$$

$$f_8 = \frac{1}{3(1 + 9 \tan^2 \varphi_i)} \left[(3 \tan \varphi_i \sin \theta_h - \cos \theta_h) e^{3(\theta_h - \theta_0) \tan \varphi_i} - 3 \tan \varphi_i \sin \theta_0 + \cos \theta_0 \right]$$

$$f_9 = \frac{1}{3} \kappa_2 \sin^2 \theta_0$$

$$f_{10} = \frac{1}{6} \kappa_1 \frac{\sin(\theta_h + \beta)}{\sin \beta} e^{(\theta_h - \theta_0) \tan \varphi_i} \left[\sin \theta_h e^{(\theta_h - \theta_0) \tan \varphi_i} + \sin \theta_0 \right]$$

$$g_1 = 2 \int_{\theta_b}^{\theta_h} \left[\left(2 f_1 f_2 + \frac{1}{2} f_2 f_3 \right) \sqrt{f_2^2 - f_3^2} + \left(f_1^2 f_2 + \frac{1}{2} f_2^3 \right) \arccos \frac{f_3}{f_2} \right] d\theta$$

$$+ 2 \int_{\theta_b}^{\theta_h} \left[\left(2 f_1 f_2 + \frac{1}{2} f_2 f_4 \right) \sqrt{f_2^2 - f_4^2} + \left(f_1^2 f_2 + \frac{1}{2} f_2^3 \right) \arccos \frac{f_4}{f_2} \right] d\theta$$

$$g_2 = \frac{b}{H} \kappa_1 \frac{e^{2(\theta_h - \theta_0) \tan \varphi_i} - 1}{2 \tan \varphi_i}$$

$$g_3 = 2 \int_{\theta_b}^{\theta_h} \left[\left(\frac{1}{8} f_2^2 f_3 - \frac{1}{4} f_3^3 - \frac{2}{3} f_1 f_3^2 - \frac{1}{2} f_1^2 f_3 + \frac{2}{3} f_1 f_3^2 \right) \sqrt{f_2^2 - f_3^2} + \left(\frac{1}{8} f_2^4 + \frac{1}{2} f_1^2 f_2^2 \right) \arccos \frac{f_3}{f_2} \right] \cos \theta d\theta$$

$$+ 2 \int_{\theta_b}^{\theta_h} \left[\left(\frac{1}{8} f_2^2 f_4 - \frac{1}{4} f_4^3 - \frac{2}{3} f_1 f_4^2 - \frac{1}{2} f_1^2 f_4 + \frac{2}{3} f_1 f_4^2 \right) \sqrt{f_2^2 - f_4^2} + \left(\frac{1}{8} f_2^4 + \frac{1}{2} f_1^2 f_2^2 \right) \arccos \frac{f_4}{f_2} \right] \cos \theta d\theta$$

$$g_4 = \frac{b}{H} \kappa_1 (f_5 - f_6 - f_7)$$

$$g_5 = 2 \int_{\theta_b}^{\theta_h} \left[\left(\frac{1}{8} f_2^2 f_3 - \frac{1}{4} f_3^3 - \frac{2}{3} f_1 f_3^2 - \frac{1}{2} f_1^2 f_3 + \frac{2}{3} f_1 f_3^2 \right) \sqrt{f_2^2 - f_3^2} + \left(\frac{1}{8} f_2^4 + \frac{1}{2} f_1^2 f_2^2 \right) \arccos \frac{f_3}{f_2} \right] \sin \theta d\theta$$

$$+ 2 \int_{\theta_b}^{\theta_h} \left[\left(\frac{1}{8} f_2^2 f_4 - \frac{1}{4} f_4^3 - \frac{2}{3} f_1 f_4^2 - \frac{1}{2} f_1^2 f_4 + \frac{2}{3} f_1 f_4^2 \right) \sqrt{f_2^2 - f_4^2} + \left(\frac{1}{8} f_2^4 + \frac{1}{2} f_1^2 f_2^2 \right) \arccos \frac{f_4}{f_2} \right] \sin \theta d\theta$$

$$g_6 = \frac{b}{H} \kappa_1 (f_8 - f_9 - f_{10})$$

$$g_7 = 2 \frac{\tan \delta \sin^2(\theta_h + \beta)}{\tan \varphi_i} e^{2(\theta_h - \theta_0) \tan \varphi_i} \int_{\theta_b}^{\theta_h} \frac{\sqrt{f_2^2 - f_4^2}}{\sin^2(\theta + \beta)} d\theta$$

$$g_8 = \frac{b}{H} \kappa_1^2 \frac{\tan \delta \sin(\theta_h + \beta)}{\tan \varphi_i \sin \beta} e^{(\theta_h - \theta_0) \tan \varphi_i}$$

$$g_9 = \sin(\beta + \delta) \left[\sin \theta_h e^{(\theta_h - \theta_0) \tan \varphi_i} - \frac{h}{H} \kappa_1 \right] - \cos(\beta + \delta) \left[\cos \theta_h e^{(\theta_h - \theta_0) \tan \varphi_i} + \frac{h}{H} \kappa_1 \cot \beta \right]$$

$$g_{10} = \frac{2 \sin(\theta_h + \beta) \sin \beta}{\kappa_1} e^{(\theta_h - \theta_0) \tan \varphi_i} \int_{\theta_b}^{\theta_h} \frac{\sqrt{f_2^2 - f_4^2}}{\sin^2(\theta + \beta)} d\theta + \frac{b}{H} \kappa_1$$